Structural Modifications Induced by Composition in the $La_{1.33-x}Na_{3x}Ti_2O_6$ Perovskites: A Neutron Diffraction Study

Ana I. Ruiz,* M. Luisa López, Carlos Pico, and M. Luisa Veiga

Departamento de Química Inorgánica I, Facultad de CC Químicas, Universidad Complutense de Madrid, 28040 Madrid, Spain

Received September 20, 2004. Revised Manuscript Received January 4, 2005

Polycrystalline samples of general composition $La_{1.33-x}Na_{3x}Ti_2O_6$ were prepared by the "liquid mix" technique. The structural analysis carried out from different techniques (XRPD, ED, HREM, and NPD) evidences that these perovskites undergo phase transformations that seem to be mainly related to the number of A-vacancies. For high degrees of substitution, x, that imply low number of vacant A-sites, a random distribution of Na^+ and La^{3+} ions in these sites is observed. When this number increases (for $x = 0.16$ and 0.11) two different cells are adopted, in which the A-cations are ordered by layers along one direction, whose dimensions are $a \approx b \approx \sqrt{2}a_p$; $c \approx 2a_p$ (space group *Pbmm*) and $a \approx b \approx c \approx 2a_p$ (space group *Cmmm*), respectively. These structural changes are analyzed on the basis of the group−subgroup relations and the tilting of the TiO_6 octahedra.

Introduction

Perovskite-type structures of general formula ABO_3 with A-cations deficiency, derived from $La_{2/3}TiO_3$, are of interest because the vacancies at these sites facilitate the electrochemical insertion of Li^+ ions and the subsequent movement of these cations through the lattice. For this parent phase $La_{2/3}TiO_3$ different structural models have been proposed. Tien and Hummel[1] recorded superlattice reflections indicative of cell doubling in more than one direction, whereas Abe and Uchino[2] and Bouwma et al.[3] found evidences for cell doubling along one direction only ($a_p \times a_p \times 2a_p$), and attributed this fact to different ionic populations (layering) on successive layers of the perovskite A-sites. On the other hand, MacEachern et al.[4] fitted neutron diffraction patterns for $La_{2/3}TiO_3$ assuming an orthorhombic structure, space group *Pban*, in a cell of dimensions $\sqrt{2}a_p \times \sqrt{2}a_p \times 2a_p$ taking into account the tilting of the TiO_6 octahedra. These models have in common a layered ordering of A-site cations, in such a way that the $z = 0$ layer is mainly occupied by La^{3+} ions and the next layer ($z = 1/2$) remains partially vacant. According to this description, one crystallographic parameter is doubled in at least one direction.

In closed related systems, such as $La_{0.6}Sr_{0.1}TiO_3$ and $La_{0.63}(Ti_{0.92}Nb_{0.08})O_3$, subtle structural changes have been reported.[5,6] Both compounds were described with double cell $2a_p \times 2a_p \times 2a_p$, in the space group *Cmmm*, and the octahedral tilting is produced about the perpendicular axis to A-site layering.

Structural modifications are expected by introducing alkaline ions, which replace some proportions of lanthanum ones to preserve the crystal electroneutrality, in the vacant A-sites giving rise to the series $La_{1.33-x}A_{3x}Ti_2O_6$. These compounds are of interest because they exhibit ionic conductivity (A = Li) and dielectric (A = Na) properties; both structural and electrical properties have been extensively investigated.[7−37] Similarly to the previous systems, different structural models have been proposed for these derivatives

* To whom correspondence should be addressed. E-mail: anairuiz@quim.ucm.es.

(1) Tien, T. Y.; Hummel, F. A. *Trans Br. Ceram. Soc.* **1969**, *66*, 233.
(2) Abe, M.; Uchino, K. *Mater. Res. Bull.* **1974**, *9*, 147.
(3) Bouwma, J.; De Vries, K. J.; Burggraaf, A. J. *Phys. Status Solidi A* **1976**, *35*, 281.
(4) MacEachern, M. J.; Dabkowska, H.; Garrett, D.; Amow, G.; Gong, W.; Liu, G.; Greedan, J. E. *Chem. Mater.* **1994**, *6*, 2092.
(5) Howard, C. J.; Zang, Z. *J. Phys.: Condens. Matter.* **2003**, *15*, 4543.
(6) Ali, R.; Yashima, M.; Tanaka, M.; Yoshioka, H.; Mori, T.; Sasaki, S. *J. Solid State Chem.* **2002**, *164*, 51.
(7) Brous, J.; Fankuchen, I.; Banks, E. *Acta Crystallogr.* **1953**, *6*, 67.
(8) Inaguma, Y.; Chen, L.; Itoh, M.; Nakamura, T. *Solid State Ionics* **1994**, *70/71*, 196.
(9) Itoh, M.; Inaguma, Y.; Jung, W.-H.; Chen, L.; Nakamura, T. *Solid State Ionics* **1994**, *70/71*, 203.
(10) León, C.; Lucía, M. L.; Santamaría, J.; París, M. A.; Sanz, J.; Várez, A. *Phys Rev. B* **1996**, *54* (1), 184.
(11) Emery, J.; Buzare, J. Y.; Bonke, O.; Fourquet, J. L. *Solid State Ionics* **1997**, *99*, 41.
(12) Lee, J.-S.; Yoo, K. S.; Kim, T. S.; Jung, H. J. *Solid State Ionics* **1997**, *98*, 15.
(13) León, C.; Santamaría, J.; París, M. A.; Sanz, J.; Ibarra, J.; Torres, L. M. *Phys. Rev. B* **1997**, *56* (9), 5302.
(14) Harada, Y.; Ishigaki, T.; Kawai, H.; Kuwano, J. *Solid State Ionics* **1998**, *108*, 407.
(15) León, C.; Lucía, M. L.; Santamaría, J.; Sánchez-Quesada, F. *Phys. Rev. B* **1998**, *57* (1), 41.
(16) Harada, Y.; Hirakoso, Y.; Kawai, H.; Kuwano, J. *Solid State Ionics* **1999**, *121*, 245.
(17) Ibarra, J.; Várez, A.; León, C.; Santamaría, J.; Torres-Martínez, L. M.; Sanz, J. *Solid State Ionics* **2000**, *134*, 219.
(18) Ivanov-Schitz, A. K.; Kireev, V. V.; Chaban, N. G. *Solid State Ionics* **2000**, *136-137*, 501.
(19) París, M. A.; Sanz, J.; León, C.; Santamaría, J.; Ibarra, J.; Várez, A. *Chem. Mater.* **2000**, *12*, 1694.
(20) Ruiz, A. I.; López, M. L.; Veiga, M. L.; Pico, C. *Solid State Ionics* **1998**, *112*, 291.
(21) Ruiz, A. I.; López, M. L.; Veiga, M. L.; Pico, C. *Int. J. Inorg. Mater.* **1999**, *1*, 193.
(22) Inaguma, Y.; Sohn, J. H.; Kim, I. S.; Itoh, M.; Nakamura, T. *J. Phys. Soc. Jpn.* **1992**, *61* (10), 3831.
(23) Nakamura, T.; Shan, Y. J.; Sun, P. H.; Inaguma, Y.; Itoh, M. *Solid State Ionics* **1998**, *108*, 53.

10.1021/cm048353a CCC: $30.25
Published on Web 02/17/2005

depending on the nature of A-cation, vacancies number, composition, and syntheses conditions.

The most studied system is $La_{1.33-x}Li_{3x}Ti_2O_6$ but precise crystal structures for different x values have not been well established until now and controversial results have been reported in the literature.[7,17,19,26−37] In any case, the proposed structural models have in common that the A-sites are occupied by alkaline and lanthanum cations and all the titanium ions are located in the B-sites. By contrast, the analogous sodium series, $La_{1.33-x}Na_{3x}Ti_2O_6$, seem to be much less studied, and only the $LaNaTi_2O_6$[7,38] and $La_{1.15}Na_{0.85}Ti_2O_6$[37] samples have been structurally characterized to our knowledge.

The adequate crystal characterization of powder specimens of these systems needs a precise determination by neutron diffraction techniques because it is certainly difficult to obtain reliable conclusions from X-ray diffraction data. This fact is related to the weakness of reflections associated with small displacements of the oxygen atoms.

The aim of this paper is to establish the crystal structure of some phases of the solid solution $La_{1.33-x}Na_{3x}Ti_2O_6$ and to follow their evolution as a function of the degree of substitution, x. This parameter obviously affects the number of A-sites occupied by cations but also their ordering among the A-layers. At the same time a complementary and interesting feature to be analyzed is the tilting of the TiO_6 octahedra that is due to slight deviations of oxygen atoms from their ideal positions. Finally, a brief theoretical analysis to establish the group−subgroup symmetry relations between the parent phase and the compounds $x = 0.11$, 0.16, and 0.28 is discussed.

Experimental Section

Polycrystalline samples of general composition $La_{1.33-x}Na_{3x}Ti_2O_6$ were prepared by the "liquid mix" technique[39] from an aqueous solution of lanthanum and sodium nitrates, $La(NO_3)_3{\cdot}6H_2O$ and $NaNO_3$, and TiO_2 in stoichiometric ratios. About 4 g of these reagents was added to a mixture of 10 g of citric acid and 4 mL of ethylene glycol. These ingredients were mixed together and drops of HNO_3 were added to catalyze the gel formation. The excess of nitric acid was boiled off and the gel was slowly decomposed by heating to 400 °C. The resulting powders were intimately mixed and heated in several steps up to temperatures ranging between 1273 and 1373 K in air for several days, in platinum crucibles. During the thermal treatment, the samples were reground in each step and the process was monitored by X-ray diffraction until single phases were obtained.

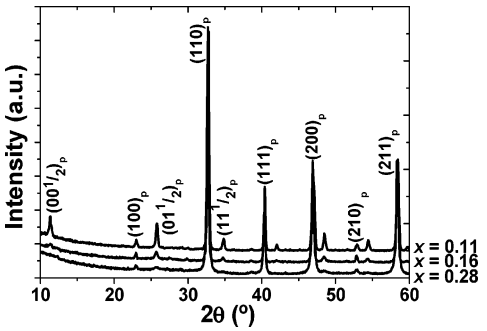

Figure 1. X-ray diffraction patterns for $x = 0.28$, 0.16, and 0.11 samples.

Chemical analyses were performed using inductive coupled plasma (ICP) spectroscopy in a JY-70 apparatus. Samples were dissolved by digestion with H_2SO_4 and $(NH_4)_2SO_4$.

X-ray powder diffraction patterns were registered by means of a Siemens Kristallofex diffractometer powered with a D-500 generator using Ni-filtered Cu Kα radiation and 2θ step size of 0.05°, with a counting time of 12.5 s for each step. The goniometer was connected to a PC controlled by the commercial program PC-APD (Analytical Powder Diffraction Software, 4.0).

Electron diffraction (ED) data and high-resolution electron microscopy (HREM) were carried out on a JEOL 400 EX microscope. Samples were prepared by dispersing ultrasonically small particles in *n*-butanol and disposing drops of this suspension on a carbon-coated copper grid.

The neutron powder diffraction data were recorded at room temperature on the D1A high-resolution powder diffractometer ($\lambda = 1.9110$ Å) at the Institut Laue-Langevin (Grenoble, France). Neutron diffraction patterns were analyzed by the Rietveld method and the Fullprof program .[40] A pseudo-Voigt function was chosen to generate the line shape of the diffraction peaks.

Results and Discussion

The synthesized samples were $La_{1.17}Na_{0.48}Ti_2O_6$ ($x = 0.16$) and $La_{1.22}Na_{0.33}Ti_2O_6$ ($x = 0.11$) in which the metal ratios were obtained by chemical analysis and compared with the phase $La_{1.05}Na_{0.84}Ti_2O_6$ ($x = 0.28$), previously described by us.[37] Structural characterization of the new materials has been performed by different diffraction techniques (X-ray, electron, and neutron).

Figure 1 shows X-ray powder diffraction patterns for the above nominal compositions of this series ($x = 0.28$, 0.16, and 0.11), in which the Bragg reflections have been indexed according to the ideal perovskite cell. Some differences are clearly observed as a function of the alkaline metal content, x. Main diffraction lines remain unchanged, but the $(0\ 0\ {}^1/_2)_p$ and $(0\ 1\ {}^1/_2)_p$ reflections arise when x decreases from the

(24) Rao, R. M. V.; Munekata, H.; Shimada, K.; Lippmaa, M.; Kawasaki, M.; Inaguma, Y.; Itoh, M.; Koinuma, H. *J. Appl. Phys.* **2000**, *88*, 6, 3756.
(25) Patil, P. V.; Chincholkar, V. S. *Curr. Sci.* **1970**, *15*, 348.
(26) Inaguma, Y.; Liquan, C.; Itoh, M.; Nakamura, T. *Solid State Commun.* **1993**, *86*, 10, 689.
(27) Belous, A. G.; Novitskaya, G. N.; Polianetskaya, S. V. *Izv. Akad. Nauk. SSSR, Neorg. Mater.* **1987**, *23* (8), 1330.
(28) Belous, A. G.; Novitskaya, G. N.; Polianetskaya, S. V.; Gornikov, Y. I. *Zh. Neorg. Khim.* **1987**, *32* (2), 283.
(29) Ruiz, A. I.; López, M. L.; Veiga, M. L.; Pico, C. *J. Solid State Chem.* **1999**, *148*, 329.
(30) Rivera, A.; León, C.; Santamaría, J.; Várez, A.; París, M. A.; Sanz, J. *J. Non-Cryst. Solids* **2002**, *307-310*, 992.
(31) García-Martín, S.; Alario-Franco, M. A.; Ehrenberg, H.; Rodriguez-Carvajal, J.; Amador, U. *J. Am. Chem. Soc.* **2004**, *126* (11), 3587.
(32) Inaguma, Y.; Katsumata, T.; Itoh, M.; Morii, Y. *J. Solid State Chem.* **2002**, *166*, 67.
(33) Sanz, J.; Alonso, J. A.; Várez, A.; Fernández-Díaz, M. T. *J. Chem. Soc., Dalton Trans.* **2002**, 1406.
(34) Sanz, J.; Várez, A.; Alonso, J. A.; Fernández-Díaz, M. T. *J. Solid State Chem.* **2004**, *177* (4−5), 1157.
(35) Fourquet, J. L.; Duroy, H.; Crosnier-López, M. P. *J. Solid State Chem.* **1996**, *127*, 283.
(36) Alonso, J. A.; Sanz, J.; Santamaría, J.; León, C.; Várez, A.; Fernández-Díaz, M. T. *Angew. Chem., Int. Ed.* **2000**, *39*, 3, 619.
(37) Ruiz, A. I.; López, M. L.; Pico, C.; Veiga, M. L. *J. Solid State Chem.* **2002**, *163*, 472.
(38) Rivera, A.; León, C.; Santamaría, J.; Várez, A.; V'yunov, O.; Belous, A. G.; Alonso, J. A.; Sanz, J. *Chem. Mater* **2002**, *14*, 5148.
(39) Pechini, M. U. S. Patent 3,330,697, 1967.
(40) Rodríguez-Carvajal, J. *Physica B* **1993**, *192*, 55.

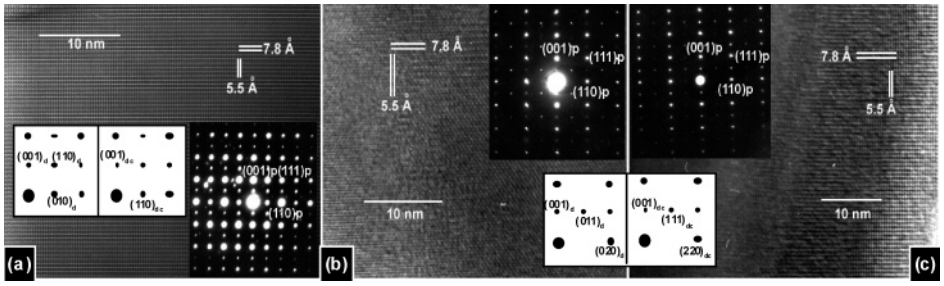

Figure 2. SAED patterns and HRTEM images corresponding to the $[\bar{1}10]_p$ zone axis for the samples (a) $x = 0.28$, (b) $x = 0.16$, and (c) $x = 0.11$. Subscripts stand for the following: p, ideal cubic cell; d, diagonal cell; dc, double orthorhombic cell.

compositional limit $x = 0.28$. These extra reflections are indicative of a supercell and can be indexed by considering either a diagonal or double cell with respect to the primitive one. The unit cell dimensions are related to the aristotype ones as follows: $a \approx b \approx \sqrt{2}a_p$ and $c \approx 2a_p$ or $a \approx b \approx c \approx 2a_p$ respectively, where a_p is the parameter of the idealized cubic perovskite cell of about 3.9 Å. In a previous work,[37] we have reported that the $x = 0.28$ specimen exhibits a diagonal cell as was deduced from electron and neutron diffraction data.

Some authors[31] have pointed out that the microstructural study is very important for determining the crystal structure of similar materials. For this reason electron diffraction and high-resolution transmission electron microscopy results are discussed first.

Figure 2 shows the ED patterns and the corresponding images along the $[\bar{1}10]_p$ zone axis for the three compositions. In the $x = 0.28$ ED pattern (Figure 2a) the $(0\ 0\ {}^1/_2)_p$, $({}^1/_2\ {}^1/_2\ 0)_p$, and $({}^1/_2\ {}^1/_2\ {}^1/_2)_p$ superlattice reflections are observed and they can be indexed on the basis of a double or a diagonal cell that are detailed in the adjacent scheme. The HRTEM images show one domain with periodicities $2a_p$ along $[001]_p$ and $\sqrt{2}a_p$ along $[110]_p$ directions. A similar situation is found for the remaining compositions ($x = 0.16$ and $x = 0.11$, Figure 2b and c, respectively) with the only difference being the absence of the $({}^1/_2\ {}^1/_2\ 0)_p$ superlattice reflection. Therefore, cells of dimensions $\sqrt{2}a_p \times \sqrt{2}a_p \times 2a_p$ or $2a_p \times 2a_p \times 2a_p$ must be considered for the three compositions.

On the other hand, Figure 3 shows the patterns corresponding to the $[001]_p$ zone axis for the samples $x = 0.16$ and 0.11, which present some relevant differences between them. Thus, for $x = 0.16$ (Figure 3a) the $(0\ 0\ {}^1/_2)_p$ and $(0\ {}^1/_2\ 0)_p$ reflections clearly appear but the $({}^1/_2\ {}^1/_2\ 0)_p$ one is absent again. The corresponding HRTEM images exhibit different kinds of domains, such as regions with $\sim 2a_p$ periodicity along the $[100]_p$ and $[010]_p$ directions and areas having a $\sim\sqrt{2}a_p$ periodicity along the $[110]_p$ direction. It can be concluded that this crystal is formed by three sets of microdomains in the $\sqrt{2}a_p \times \sqrt{2}a_p \times 2a_p$ cell with the c axis orientated along one of the three main crystallographic directions in each domain set. These results for the $x = 0.28$ and 0.16 samples agree well with those previously obtained by us by neutron diffraction techniques.[37] Nevertheless, the $x = 0.11$ ED pattern shows extra reflections on $({}^h/_2\ {}^k/_2\ 0)_p$ (Figure 3b), and the corresponding HRTEM image along the $[001]_p$ zone axis only presents one domain with $2a_p$ periodicity that suggests a unit cell of parameters $2a_p \times 2a_p \times 2a_p$.

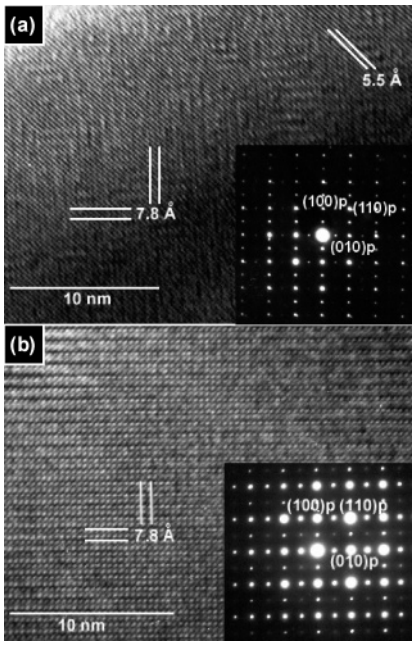

Figure 3. SAED patterns and HRTEM images corresponding to the $[001]_p$ zone axis for the samples (a) $x = 0.16$; and (b) $x = 0.11$.

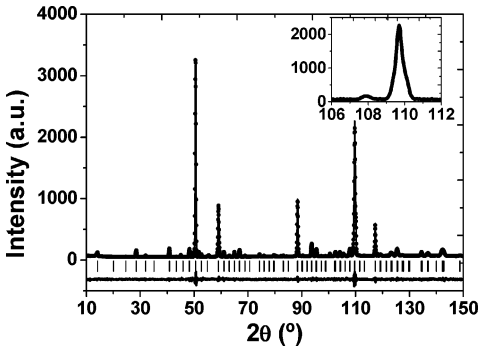

Figure 4. Experimental, calculated, and difference neutron diffraction patterns for the sample $x = 0.16$. The inset shows a magnification of the zone $2\theta = 106-112°$.

Therefore, the compounds $La_{1.05}Na_{0.84}Ti_2O_6$ (i.e., $x = 0.28$) and $La_{1.17}Na_{0.48}Ti_2O_6$ (i.e., $x = 0.16$) show the same diagonal basic unit cell ($\sqrt{2}a_p \times \sqrt{2}a_p \times 2a_p$), but a double unit cell ($2a_p \times 2a_p \times 2a_p$) seems to be more adequate to describe the oxide $La_{1.22}Na_{0.33}Ti_2O_6$ (i.e., $x = 0.11$). Both latter phases exhibit the $(0\ 0\ {}^l/_2)_p$ reflections, for which $l = 2n + 1$, that can be related to an ordering of the La and Na ions and vacancies within the A-sites.

The respective powder neutron diffraction patterns of $x = 0.16$ and $x = 0.11$ samples are shown in Figures 4 and 5. Besides the superlattice reflections, due to the alternative

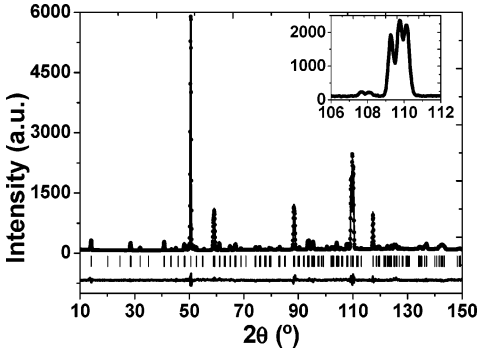

Figure 5. Experimental, calculated, and difference neutron diffraction patterns for the sample $x = 0.11$. The inset shows a magnification of the $2\theta = 106-112°$ zone.

arrangement of La and Na ions and vacant sites along the *c*-axis,[37] additional extra peaks were detected. All of them could be indexed in a diagonal cell for both compounds. Nevertheless, the intense $(311)_p$ reflection that appears at $2\theta \approx 110°$ is clearly split in three components for $x = 0.11$ but is unique for $x = 0.16$ (see insets in Figures 4 and 5). Taking into account this feature it is evident that the pattern corresponding to $La_{1.22}Na_{0.33}Ti_2O_6$ must be indexed using a double unit cell, i.e., a ($\approx 2a_p$) $\times$ b ($\approx 2a_p$) $\times$ c ($\approx 2a_p$) instead of the diagonal one that is more appropriate for $La_{1.17}Na_{0.48}Ti_2O_6$.

The structures of $La_{0.55}Li_{0.35}TiO_3$[26] and $La_{0.62}Li_{0.16}TiO_3$[27] were chosen as trial models for fitting the neutron diffraction patterns of $x = 0.16$ and $x = 0.11$, respectively. The observed and calculated patterns as well as the differences between them using the *Pbmm* space group for $x = 0.16$ and the *Cmmm* one for $x = 0.11$ are also shown in Figures 4 and 5. Structural parameters, agreement factors, and isotropic factors for La, Na, Ti, and O are given in Table 1. The agreement factors, R_B, R_p, and R_{wp}, are lower than 5, 6, and 7%, respectively, and such refinements confirm the validity of the corresponding structural models. In conclusion, La and Na ions and the vacancies are located on the highest coordination A-sites and Ti atoms are on the octahedral B-sites. The occupancy of the A-sites is consistent with the chemical formulas for both samples and shows the sequence of nearly occupied planes ($z = 0$, $N \approx 0.95$). These planes alternate along the *c*-axis with those containing the remaining La/Na atoms and vacancies ($z = 0.5$). By contrast, in the $x = 0.28$ sample where the number of vacancies is practically negligible, the vacancies and La/Na cations are distributed at random in the above-mentioned A-sites (the corresponding data are included in Table 1 for comparison).

With regard to the location of Ti atoms in these ordered structures (*Cmmm* and *Pbmm*), the atomic coordinate along the ordering axis is ~0.26 showing that these cations are slightly displaced from their ideal position ($z = {}^1/_4$) toward the upper [La/Na[2]]−O2 layer. The cation deficiency in such a layer ($z = 0.5$) provokes an excess of negative charge that is compensated by the approach of highly charged Ti^{4+} cations. The *z* atomic coordinates of O3 and O5 for the *Cmmm* structure and O4 for the *Pbmm* one vary between 0.21 and 0.23, showing that these atoms are displaced downward from their ideal positions to the La/Na nearly occupied layer with relative excess of positive charge. These

Table 1. Refined Atomic Positions, Occupation for La and Na Ions, Isotropic Temperature Factors (in Å²), Cell Constants (in Å), and R-factors for $La_{1.33-x}Na_{3x}Ti_2O_6$

		$x = 0.11$	$x = 0.16$	$x = 0.28$
		Cmmm	*Pbmm*	*Ibmm*
(La/Na)1	*x*	0.00	0.7453(5)	0.0019(1)
	y	0.2530(1)	0.25	0.0000
	z	0.00	0.00	0.2500
	N	0.94(2)/0.01(2)	0.83(4)/0.12(1)	1.05/0.84
	β	0.12(3)	0.39(6)	0.97(4)
(La/Na)2	*x*	0.00	0.7614(8)	
	y	0.2576(3)	0.25	
	z	0.50	0.50	
	N	0.28(5)/0.32(1)	0.34(2)/0.36(1)	
	β	1.12(5)	1.16(5)	
Ti	*x*	0.2471(6)	0.2560(1)	0.0000
	y	0.00	0.25	0.5000
	z	0.2604(3)	0.2574(4)	0.0000
	β	0.32(5)	0.39(4)	0.82(8)
O1	*x*	0.2727(2)	0.2102(1)	0.0452(2)
	y	0.00	0.25	0.5000
	z	0.00	0.00	0.2500
	β	0.78(2)	0.92(1)	1.52(1)
O2	*x*	0.2269(4)	0.2863(4)	0.7500
	y	0.00	0.25	0.2500
	z	0.50	0.50	0.0238(5)
	β	1.16(5)	1.47(5)	1.38(7)
O3	*x*	0.00	0.00	
	y	0.00	0.00	
	z	0.2117(2)	0.7446(5)	
	β	0.70(1)	0.88(1)	
O4	*x*	0.00	0.50	
	y	0.50	0.00	
	z	0.2635(4)	0.7747(5)	
	β	0.77(4)	0.87(5)	
O5	*x*	0.25		
	y	0.25		
	z	0.2367(5)		
	β	0.57(4)		
	a	7.7234(2)	5.4766(2)	5.4798(2)
	b	7.7485(2)	5.4763(4)	5.4753(4)
	c	7.7803(3)	7.7624(5)	7.7432(5)
	R_B	3.52	4.58	1.83
	R_P	4.97	5.68	4.62
	R_{WP}	6.73	6.89	5.83

oxygen displacements are also responsible for distortions in the TiO_6 octahedra in which two longer and two shorter Ti−O distances with respect to the mean values were deduced along the *c*-axis. Table 2 gathers these distances labeled as Ti−O1 and Ti−O2 for $x = 0.11$ (*Cmmm*) and 0.16 (*Pbmm*), respectively. Such distortions were not observed for the $x = 0.28$ derivative where a random distribution of La^{3+} and Na^+ cations was found. The average of Ti−O interatomic lengths scarcely varies from 1.947 to 1.949 Å, and they are in good agreement with the Shannon ionic radii sums.[41] To study the TiO_6 octahedra distortion, the O−Ti−O angles have been calculated, giving different deviations from the ideal cubic perovskite (90° angle) as far as 6° for the A-ordered phases (*Cmmm* and *Pbmm*), whereas the deviation is ±0.4° for the remaining one (*Ibmm*).

Table 2 also includes the A−O interatomic distances for the title compounds that are compared with the expected ones from the Shannon ionic radii. These results suggest that lanthanum and sodium cations are located on distorted 12-coordinated polyhedra in which interatomic distances vary over a wide range (between 3.0 and 2.6 Å), although the mean A−O lengths are of the same order as the expected

(41) Shannon, R. D. *Acta Crystallogr. A* **1976**, *32*, 751.

Table 2. Main Interatomic Distances (in Å) and Angles (deg) for $La_{1.33-x}Na_{3x}Ti_2O_6$

	Cmmm ($x = 0.11$)	*Pbmm* ($x = 0.16$)	*Ibmm* ($x = 0.28$)
d [(La/Na)1−O1]	2.877(1) × 2	2.930(4)	2.998(3)
	2.597(4) × 2	2.749(1) × 2	2.74(1) × 2
		2.546(2)	2.482(5)
d [(La/Na)1−O2]			2.866(8) × 4
			2.617(3) × 4
d [(La/Na)1−O3]	2.560(3) × 2	2.784(1) × 4	
d [(La/Na)1−O4]	2.805(2) × 2	2.596(7) × 4	
d [(La/Na)1−O5]	2.669(7) × 4		
d [(La/Na)2−O2]	2.656(2) × 2	2.875(1)	
	2.824(3) × 2	2.751(5) × 2	
		2.602(4)	
d [(La/Na)2−O3]	3.002(3) × 2	2.681(1) × 4	
d [(La/Na)2−O4]	2.630(7) × 2	2.911(4) × 4	
d [(La/Na)2−O5]	2.815(4) × 4		
d [(La/Na)1−O] mean	2.695	2.708	2.742
d [(La/Na)2−O] mean	2.790	2.779	
d [(La/Na)−O] mean	2.743	2.743	2.742
Shannon	2.77	2.77	2.77
d (Ti−O1)	2.035(2)	2.014(3)	1.952(2) × 2
d (Ti−O2)	1.871(1)	1.890(1)	1.945(6) × 4
d (Ti−O3)	1.945(2)	1.959(2) × 2	
d (Ti−O4)	1.954(4)	1.930(1) × 2	
d (Ti−O5)	1.946(5) × 2		
d (Ti−O) mean	1.949	1.947	1.947
Shannon	2.00	2.00	2.00
ϕ^- angle	5.2	6.2	7.3
		4.9	5.5
O1−Ti−O2			89.7 × 4
			90.3 × 4
O1−Ti−O3	84.4	84.4 × 2	
O1−Ti−O4	85.1	87.6 × 2	
O1−Ti−O5	84.5 × 2		
O2−Ti−O2			90.3 × 2
			89.4 × 2
O2−Ti−O3	96.4	94.1 × 2	
O2−Ti−O4	94.1	93.9 × 2	
O2−Ti−O5	95.4 × 2		
O3−Ti−O3		88.6	
O3−Ti−O4		89.9 × 2	
O3−Ti−O5	89.6 × 2		
O4−Ti−O4		90.4	
O4−Ti−O5	89.4 × 2		

ones. The different degree of cation occupancy in the La/Na layers is the cause of the two different kinds of A-polyhedra, $[La/Na^1]O_{12}$ and $[La/Na^2]O_{12}$ found in *Cmmm* and *Pbmm* cells, whose mean A−O distances are 2.7 and 2.8 Å, respectively.

To visualize the distinctive features found in this series, Figure 6 gives a nonconventional picture of the TiO_6 and $(La/Na)O_{12}$ frameworks separately for these derivatives. Starting from the more regular *Cmmm* space group that describes the phase $x = 0.11$, one can see that $La(1)O_{12}$ and $[La/Na(2)]O_{12}$ polyhedra alternate in the *ac*-plane above and below the TiO_6 octahedra (Figure 6a). An interesting point to be noted is the relatively high difference between the A−O interatomic distances. The O5 and O3 atoms are clearly displaced toward the La(1) atoms (2.66 and 2.56 Å, respectively) and moved away from the La/Na-(2) ones (2.81 and 3.02 Å, respectively). As a consequence of the octahedral tilting, the A−O4 distances are of the same order as the A−O5 ones but in the opposite sense. In this respect, the mean distances at these four equatorial oxygen atoms indicate that they are nearer to the La^1 plane than to the plane built by $La_{0.28}Na_{0.32}\square_{0.4}$. Therefore, the TiO_6 tilting around the A-sites provokes a zigzag arrangement of apical oxygen atoms in the *ac*-plane and the *Cmmm* cell has an antiphase tilting along the *b*-axis [$a^0b^-c^0$ in Glazer's notation[42,43]].

Similarly, Figure 6b shows a structural scheme for the $x = 0.16$ sample. Note that TiO_6 octahedra plane runs along the *ab*-diagonal of the primitive cell as well as the tilting associated to the scheme $a^-b^0c^-$. With respect to the $(La/Na)O_{12}$ polyhedra (Figure 6b), the difference between the shortest and longest A−O interatomic distances diminishes because of the higher content of La^{3+} and Na^+ cations in the $z = 0.5$ plane. For instance, the highest [La/Na(2)]−O3 bond length in the *Cmmm* was 3.02 Å and now is 2.91 Å (to O4 in *Pbmm*), and the [La/Na(1)]−O3 one was 2.56 Å and changes to 2.59 Å in this diagonal structure.

To complete the structural evolution with composition in this series, it is interesting to compare the above results with those of the limit phase ($x = 0.28$, space group *Ibmm*), depicted in Figure 6c. Recalling that the La/Na planes have similar atomic contents and there is a random distribution of both elements on them, the corresponding polyhedra are identical. Therefore, interatomic A−O2 distances are of 2.61 and 2.86 Å, closer than in the previous cases. Both distances alternate with respect to the upper and lower A-planes. In this case the octahedra tilting ($a^-b^0c^-$) is the same as that in *Pbmm*.

Table 2 shows the tilt angles, calculated by using the refined crystal parameters, decrease (7.3° to 6.2° to 5.2°) as the vacant A-sites increase. The octahedra tiltings were estimated from the inclination of apical oxygen atoms (O1 and O2 for *Cmmm* and *Pbmm*, and O1 for *Ibmm*) with respect to the *c*-axis. Moreover, a second tilt angle is found in the diagonal cells, because they are consistent with a two-axis tilt system, and this angle also decreases (5.5° to 4.9°) in the same sense as before.

In conclusion, the structural characteristics of this perovskite-type series, in particular the cation order−disorder phenomena on the A-sites and the BO_6 octahedra tilting, seem to be related to the vacant A-sites number. When vacancies increase, the octahedra tilting decreases and the 12-coordination hole in the $z = 0.5$ plane is bigger than that in the $z = 0$ one. This conclusion is supported by the phase $La_{0.64}Ti_{0.92}Nb_{0.08}O_3$, described as an orthorhombic double cell.[44] In this phase the number of vacant A-sites is higher than in ours and shows a smaller octahedra tilting (4.7°).

As a hypothesis, these facts could be related to the well-known features in the ReO_3 and $CaTiO_3$ types. In the first structure type all the A-cation sites are vacant and the void defined by oxygen atoms is a regular cuboctahedron. In the perovskite-like structure of $CaTiO_3$ all the A-sites are occupied but oxygen atoms are displaced from their ideal positions and the coordination number of Ca^{2+} is 8; as a consequence, the TiO_6 octahedra show a tilting angle of 10°. In our system $La_{1.33-x}Na_{3x}Ti_2O_6$ we have intermediate situations with respect to the number of vacancies in the A-sites. For the composition $x = 0.28$ this number is

(42) Glazer, A. M. *Acta Crystallogr. B* **1972**, *28*, 3384.
(43) Glazer, A. M. *Acta Crystallogr. A* **1975**, *31*, 756.
(44) Yashima, M.; Mori, M.; Kamiyama, T.; Oikawa, K.; Hoshikawa, A.; Torii, S.; Saitoh, K.; Tsuda, K. *Chem. Phys. Lett.* **2003**, *375*, 240.

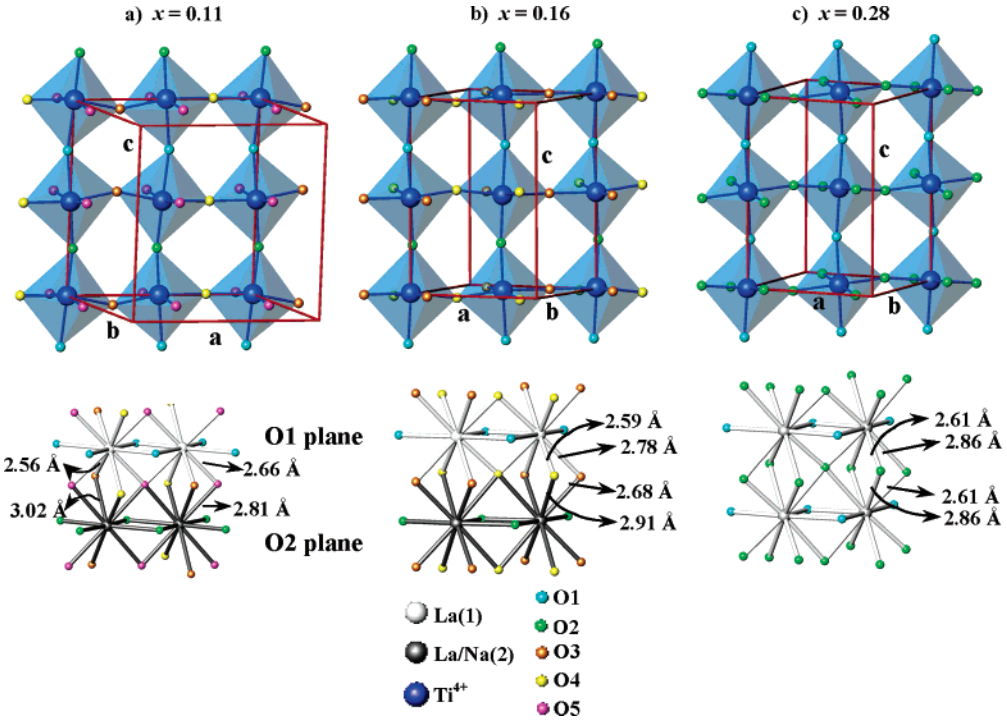

Figure 6. Cation polyhedra arrangements for (a) $x = 0.11$; (b) $x = 0.16$; and (c) $x = 0.28$. Upper graphs refer to BO_6 octahedra and lower graphs stand for AO_{12} polyhedra.

Scheme 1. Structural and Group−Subgroup Relationships of $La_{1.33-x}Na_{3x}Ti_2O_6$, Starting from the Parent Cubic Aristotype

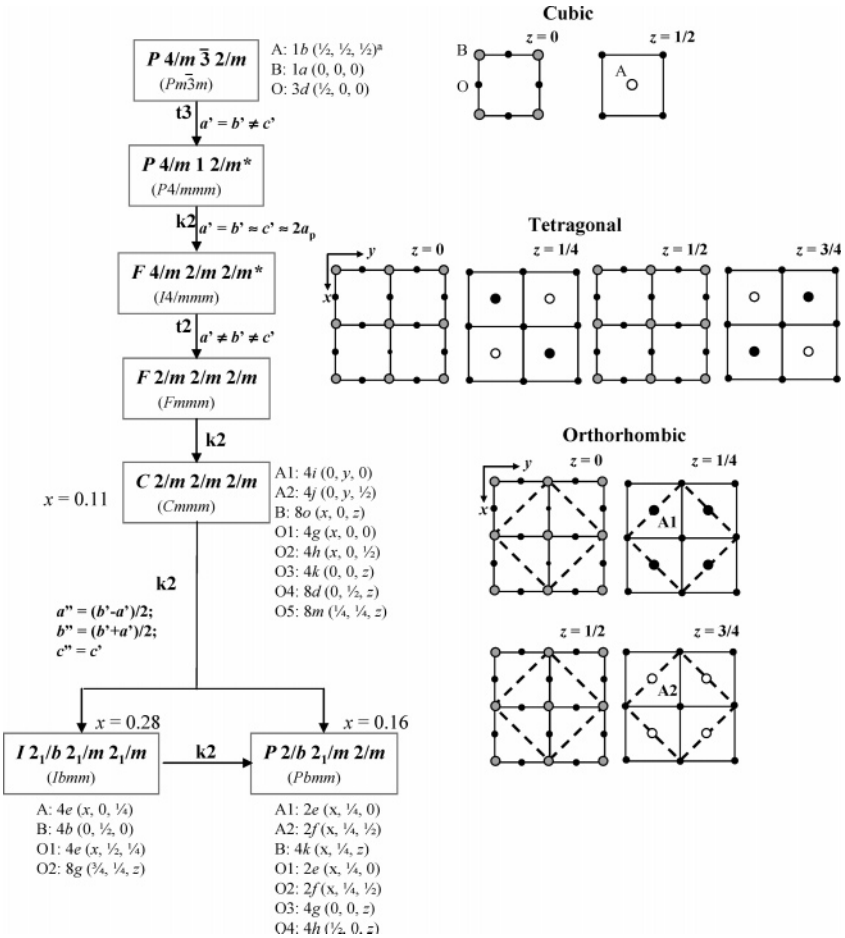

*Non conventional symbol. [a] Wyckoff site labels and atomic coordinates for A, B, and O ions.

low and the unique effect is the TiO_6 octahedra tilting, analogous to the case of $CaTiO_3$. When the number of vacant A-sites increases, these are concentrated on alternate planes together with sodium cations and we can imagine that

pseudo-planes of "ReO_3"- and "$CaTiO_3$"-types are superposed along the *c*-direction. Therefore, the tilting angle of TiO_6 octahedra could be progressively reduced as the degree of substitution, *x*, diminishes because the "right" ReO_3-like pseudo-planes exert a more predominant effect on the above tilting.

Overview of Symmetry Relations

The above-discussed structural relations in the title system as well as the oxygen displacements can be better understood by taking into account some symmetry arguments. Different structural analyses in perovskite-type compounds attract great attention in order to establish adequate relationships between crystal structure and properties. Following the ideas of Thomas[45] and Müller,[46] and according to Hermann's theorem,[47] Scheme 1 shows group−subgroup relationships in our system starting off with the parent cubic aristotype, *Pm*3*m*. Next to Scheme 1 the main structural features and the most representative idealized structures are depicted.

The transformation to tetragonal *P*4/*mmm* group is accomplished by the disappearance of the 3-fold axes, and the new lattice parameters must vary according to the change in symmetry (noted on the arrow: $\boldsymbol{a}' = \boldsymbol{b}' \neq \boldsymbol{c}'$). This process implies that the maximal nonisomorphic subgroup is "*translationengleich*" of index 3 (i.e., ***t3***). The second step in this family tree involves an enlargement of the unit cell by a ***k2*** operator that preserves the tetragonal symmetry, giving rise to the *F4/mmm* nonconventional symbol. A further ***t2*** transformation leads to the *Fmmm* maximal nonisomorphic subgroup. However, this space group is not compatible with the experimental systematic extinctions ($h + k = 2n + 1$) that suggest a face-centered *C*-type lattice. According to that, the following step is the ***k2*** transformation to *Cmmm* space group, giving as a result a reduction in the centering of the new cell. From this latter orthorhombic group two different ***k2*** transformations give rise to the searched *Ibmm* and *Pbmm* space groups (which are obviously also related by ***k2*** operator). The relations between the parameters of these orthorhombic space groups are shown in Scheme 1 where the new cell is depicted in dotted lines.

This theoretical group−subgroup study is linked with the three structural degrees of freedom in perovskite-type derivatives[45] and clarifies the experimental tendency to higher tiltings of BO_6 octahedra as the vacant A-sites decreases. In the title compounds the A-cations exhibit a quite distorted cuboctahedral coordination that is compatible with the relative size of the ions implied in such structures. As stated above, this distortion is a consequence of displacements of oxygen anions that provoke the tilting of BO_6 octahedra.

Conclusions

Neutron diffraction data and complementary electron microscopy techniques allowed to us to establish without ambiguity the structural changes governed by stoichiometry in the perovskites $La_{1.33-x}Na_{3x}Ti_2O_6$.

On the other hand, the analysis carried out by means of group−subgroup relations explains how slight variations in composition produce displacements in the oxygen atoms that lead to different space groups. Thus, the $x = 0.11$ sample shows a double orthorhombic cell (space group *Cmmm*) whereas the $x = 0.16$ and 0.28 ones present diagonal orthorhombic cells whose space groups are *Pbmm* and *Ibmm*, respectively.

Finally, *Cmmm* and *Pbmm* phases are built by layers of La and Na/vacancies that are alternately occupied and partly occupied along the *c*-axis. Titanium atoms move from their ideal sites toward the Na/vacancy-rich layer. However, A-cations (La and Na) and A-vacancies are distributed at random in *Ibmm* cell, in which Ti cations are located in fixed special sites.

Acknowledgment. We appreciate the financial support of the CICYT (MAT2002-01288) and (MAT2003-06003-C02-02). A.I.R. is grateful to the Comunidad de Madrid for a postdoctoral fellowship. We appreciate the technical assistance of Dr. M. T. Fernández-Díaz and the ILL for collecting data of neutron diffraction. We thank the C.A.I. of X-ray Diffraction and the Electron Microscopy "Luis Brú" from UCM.

CM048353A

(45) Thomas, N. W. *Acta Crystallogr. B* **1998**, *54*, 585.
(46) Müller, U. *Inorganic Structural Chemistry*; Wiley: New York, 1993.
(47) Hermann, C. *Z. Kristallogr.* **1929**, *69*, 533.